Author Manuscript

Author Manuscript

Author Manuscript

Author Manuscript

HHS Public Access

Author manuscript

Cardiovasc Eng Technol. Author manuscript; available in PMC 2024 December 18.

Published in final edited form as:

Cardiovasc Eng Technol. 2024 December ; 15(6): 760–774. doi:10.1007/s13239-024-00752-z.

Deforming Patient-Specific Models of Vascular Anatomies to Represent Stent Implantation via Extended Position Based Dynamics

Jonathan Pham[1], **Fanwei Kong**[2], **Doug L. James**[3], **Jeffrey A. Feinstein**[2,4], **Alison L. Marsden**[2,4,*]

[1]Department of Mechanical Engineering, Stanford University, Stanford, CA, USA.

[2]Department of Pediatrics, Stanford University, Stanford, CA, USA.

[3]Department of Computer Science, Stanford University, Stanford, CA, USA.

[4]Department of Bioengineering, Stanford University, Stanford, CA, USA.

Abstract

Purpose: Angioplasty with stent placement is a widely used treatment strategy for patients with stenotic blood vessels. However, it is often challenging to predict the outcomes of this procedure for individual patients. Image-based computational fluid dynamics (CFD) is a powerful technique for making these predictions. To perform CFD analysis of a stented vessel, a virtual model of the vessel must first be created. This model is typically made by manipulating two-dimensional contours of the vessel in its pre-stent state to reflect its post-stent shape. However, improper contour-editing can cause invalid geometric artifacts in the resulting mesh that then distort the subsequent CFD predictions. To address this limitation, we have developed a novel shape-editing method that deforms surface meshes of stenosed vessels to create stented models.

Methods: Our method uses physics-based simulations via Extended Position Based Dynamics to guide these deformations. We embed an inflating stent inside a vessel and apply collision-generated forces to deform the vessel and expand its cross-section.

Results: We demonstrate that this technique is feasible and applicable for a wide range of vascular anatomies, while yielding clinically compatible results. We also illustrate the ability to parametrically vary the stented shape and create models allowing CFD analyses.

Conclusion: Our stenting method will help clinicians predict the hemodynamic results of stenting interventions and adapt treatments to achieve target outcomes for patients. It will also enable generation of synthetic data for data-intensive applications, such as machine learning, to support cardiovascular research endeavors.

*Corresponding author(s): amarsden@stanford.edu;.

Declarations

Conflicts of Interest. The authors declare that they have no conflicts of interest.

Author Manuscript Author Manuscript Author Manuscript Author Manuscript

Keywords

patient-specific cardiovascular modeling; shape editing; stents; position based dynamics; computational fluid dynamics

1 Introduction

Cardiovascular diseases are the leading cause of death in the United States [1]. They include a large range of acquired and congenital diseases, such as coronary heart and peripheral artery diseases and Alagille and Williams Syndromes. While varying in etiology, stenotic blood vessels represent a common structural abnormality among these diseases. These narrowed vessels often cause downstream changes in perfusion and elevated upstream blood pressures. Surgical or percutaneous interventions are commonly performed in these vessels to restore blood flow. However, despite numerous clinical advances in treatment strategies, predicting changes in the outcomes prior to treatment remains challenging.

Angioplasty with stenting is a minimally invasive percutaneous procedure used to improve blood flow in obstructed vessels. However, despite being one of the dominant strategies to treat various conditions, stenting is not guaranteed to achieve clinically desired outcomes. For example, it may fail to provide enough relief to achieve hemodynamic targets, such as reduced right ventricular pressures in Williams Syndrome patients with stenotic pulmonary arteries [2] or sufficient fractional flow reserve in patients with coronary artery disease [3]. In other patients, in-stent restenosis may develop [4, 5], where local hemodynamic factors, such as wall shear stress, have been found to play a contributing role [6]. Therefore, assessing the possible hemodynamic outcomes of stent placement before the procedure is performed will help clinicians mitigate unnecessary risk and unintended complications and ultimately improve outcomes.

Image-based computational fluid dynamics (CFD) modeling of patient-specific vasculature provides predictive capabilities for pre-treatment assessment in an inexpensive and risk-free manner [7]. This allows clinicians to test various treatment options in advance of a procedure and assess hemodynamic responses in a noninvasive fashion. Clinicians could personalize the procedure and create a treatment plan, including, for example, stent configuration, that yields the best hemodynamic outcomes for each specific patient [8, 9].

To perform image-based CFD modeling of a patient's vasculature, clinicians must first acquire medical images of the vessels of interest [10]. Pathlines tracing the centerlines of the vascular lumen are then created. Traversing these pathlines, two-dimensional contours outlining the lumen cross-section are then segmented. These segmentations are subsequently lofted together to create a three-dimensional surface mesh approximating the vessel shape. The surface mesh is used to create a volume mesh for CFD simulations. Boundary conditions are prescribed thereafter, and simulations can then be performed to predict hemodynamic quantities of interest, such as flow rates, pressures, and wall shear stresses.

This image-based pipeline can be used to create models reflecting the shape of the vessels prior to stent implantation. For predictive applications where stenting has not yet been

Author Manuscript Author Manuscript Author Manuscript Author Manuscript

performed in the clinic or for retrospective modeling studies without postoperative medical scans [11], the preoperative model must be modified to reflect the anticipated stented shape. The standard procedure for modifying the shape of a model involves editing the segmentations to represent the stented lumen. An extensive prescription of the stented vessel shape is often needed here to build the corresponding surface mesh. Furthermore, the contours must be carefully edited to ensure that the final segmentations can be correctly lofted. In particular, the individual contours on a vessel branch must not overlap and the contours of a daughter branch must be fully embedded within the contours of a parent branch. If these requirements are not met, the segmentations cannot be lofted or the generated surface mesh will yield geometric artifacts that affect the validity of the CFD results. For example, in Figure 1, false cap faces representing vessel outlets resulted from lofting daughter-branch segmentations that were not fully embedded within the stented branch contours. To prevent such erroneous model artifacts, the contours must generally be edited by hand. This process can be quite tedious. The difficulty of guaranteeing proper contours for subsequent lofting operations makes scripting automated segmentation-editing routines to create valid postoperative models challenging.

Existing attempts to circumvent the limitations of segmentation editing involve editing the vessel surface mesh instead. For example, SURGEM is a platform that allows clinicians to modify a vessel mesh to represent the stented shape [12]. However, it requires clinicians to manually draw an approximate centerline of a stenotic vessel branch to determine the location of the stent placement. The stenosis is inflated by “pushing” the mesh nodes approximately in the direction normal to the centerline of the branch. This limits its ability to adequately stent stenoses near multibranch junctions, which can have multiple centerline directions.

Another shape-editing framework that can be used to perform stenting is morphMan [13]. morphMan morphs vascular models by editing an implicit surface representation of the vessel mesh. However, this tool can require extensive prescription of the final stented shape to create a smoothly deformed vessel. Specifically, the cross-sectional areas at every point along the stented vessel centerline need to be prescribed, including those at centerline points corresponding to the “transition” zone around the ends of the stent where it interfaces with the native vessel. In contrast, our method only requires prescribing the location, diameter, and length of the stent to produce a physics-driven estimation of the stented vessel shape.

An alternative method to mimic stent placement is to simply inflate the stenosed region of the mesh. Various methods have been developed for such operations [14–16]. However, these techniques yield inflations with spherical-like shapes that reflect the shapes of aneurysms rather than cylindrical-like shapes, which are needed to represent the intrinsic shapes of stents.

To address the limitations of segmentation editing and previous shape-editing frameworks, we develop a method to deform the surface mesh of a preoperative model to create a postoperative, stented model. Our method allows a user to edit patient-specific models from a variety of vascular anatomies, including aortic, pulmonary, and femoral anatomies. We leverage soft-body simulations with Extended Position Based Dynamics (XPBD), an

Author Manuscript Author Manuscript Author Manuscript Author Manuscript

algorithm developed by the computer graphics industry for simulating deformable objects in animation and video games [17], to guide the shape-editing process and create shape edits that morph the stenosed mesh geometry into a plausible stented geometry. XPBD, a particle-based technique, is becoming increasingly employed for surgical simulations, such as keyhole neurosurgery [18] and heart valve repair [19]. We use XPBD to deform the vessels and expand the lumen as a stent placed inside inflates and collides with the vessel walls. Our XPBD-based approach incorporates physical information to predict more realistic stented vessel shapes compared to manual segmentation editing, while being more computationally efficient than higher fidelity numerical methods, e.g., finite element approaches. This enables us to efficiently generate clinically realistic estimations of stented vessel shapes to explore a range of treatment scenarios.

2 Methods

2.1 Soft Constraints for Deformation Modeling

In many particle-based simulation methods, like XPBD, the mechanical behavior of deformable objects is modeled through special "behavior" functions that govern the desired physical properties of interest [20, 21]. These functions are referred to as "constraints" in XPBD literature [17, 22]. They are used to define spring-like potential energies that, in turn, define the forces to be applied to the particles. The energy for a single constraint, $C(\boldsymbol{x})$, is $E(\boldsymbol{x}) = \frac{1}{2}\alpha^{-1}C(\boldsymbol{x})^2$, where the constraint is dependent on the position, $\boldsymbol{x}$, of the relevant particle; α is an inverse spring stiffness for the constraint. The force corresponding to this potential energy is $\boldsymbol{f}(\boldsymbol{x}) = -\frac{\partial E(\boldsymbol{x})}{\partial \boldsymbol{x}}$.

Three popular constraints used in XPBD are distance, dihedral bending, and attachment constraints. Distance and bending constraints are commonly employed jointly to model membranous objects, such as cloth and biological tissues [19, 22, 23]. Distance constraints control mesh edge lengths, while bending constraints control the amount of bending between adjacent cells on a triangulated mesh (Figure 2). The equations for the distance and bending constraints are

$$C_{distance}(\boldsymbol{x}_1, \boldsymbol{x}_2) = \|\boldsymbol{x}_1 - \boldsymbol{x}_2\|_2 - d_0, \tag{1}$$

$$C_{bending}(\boldsymbol{x}_1, \boldsymbol{x}_2, \boldsymbol{x}_3, \boldsymbol{x}_4) = \cos^{-1}(\boldsymbol{n}_1 \cdot \boldsymbol{n}_2) - \theta_0, \tag{2}$$

respectively, where d_0 is the rest length of the distance constraint, which is analogous to the rest length of a Hookean spring, and θ_0 is the rest angle of the bending constraint. $\boldsymbol{n}_1$ and $\boldsymbol{n}_2$ are the unit normal vectors for the associated triangle cells, where the normal vector for a triangular cell can be obtained from its three vertices. Attachment constraints bound a

Author Manuscript Author Manuscript Author Manuscript Author Manuscript

particle to a specific position, such that $C_{attachment}(\boldsymbol{x}) = \boldsymbol{x} - \boldsymbol{p}$, where $\boldsymbol{p}$ is the position that the particle is fixed to.

For simulations involving multiple entities, collision constraints are needed. Vertex-normal collision constraints are often used for collisions between particles and objects [22] (Figure 3). A vertex-normal collision constraint for a particle, $\boldsymbol{x}$, is given by

$$C_{collision}(\boldsymbol{x}) = (\boldsymbol{x} - \boldsymbol{x}_c) \cdot \boldsymbol{n}_c - d_c, \tag{3}$$

where $\|\boldsymbol{x} - \boldsymbol{x}_c\|$ is the distance between the particle and the collision point, $\boldsymbol{x}_c$, on the object; $\boldsymbol{n}_c$ is the unit normal vector of the object at this point and d_c is the minimum rest distance between the two objects. Vertex-normal collision constraints, and other collision constraints, are generally only added to an XPBD simulator when $\|\boldsymbol{x} - \boldsymbol{x}_c\| < d_c$.

2.2 Extended Position Based Dynamics

XPBD models deformable objects by representing them as collections of particles and simulating their motion according to Newton's 2nd law [17, 23]. The dynamics for a single particle, i, is given by

$$m_i \frac{d^2 \boldsymbol{x}_i}{dt^2} = \boldsymbol{f}_i\left(\boldsymbol{x}_1, \ldots, \boldsymbol{x}_i, \ldots, \boldsymbol{x}_{N_p}\right), \tag{4}$$

where $\boldsymbol{x}_i \in \mathbb{R}^3$ is the position of the particle, m_i is the mass of the particle, and $\boldsymbol{f}_i\left(\boldsymbol{x}_1, \ldots, \boldsymbol{x}_i, \ldots, \boldsymbol{x}_{N_p}\right) \in \mathbb{R}^3$ is the force applied to the particle. The force is written as a function of all N_p particles in the system for generality. The collective equation of motion for all particles is

$$\boldsymbol{M} \frac{d^2 \boldsymbol{X}}{dt^2} = \boldsymbol{F}(\boldsymbol{X}). \tag{5}$$

Here, $\boldsymbol{X} = [\boldsymbol{x}_1^T, \ldots, \boldsymbol{x}_i^T, \ldots, \boldsymbol{x}_{N_p}^T]^T \in \mathbb{R}^{3N_p}$, $\boldsymbol{F}(\boldsymbol{X}) = \left[\boldsymbol{f}_1^T(\boldsymbol{X}), \ldots, \boldsymbol{f}_i^T(\boldsymbol{X}), \ldots, \boldsymbol{f}_{N_p}^T(\boldsymbol{X})\right]^T \in \mathbb{R}^{3N_p}$, and $\boldsymbol{M} = \boldsymbol{m} \otimes \boldsymbol{I} \in \mathbb{R}^{3N_p \times 3N_p}$, where $\otimes$ is the Kronecker product, $\boldsymbol{I}$ is the 3×3 identity matrix, and $\boldsymbol{m}$ is a diagonal matrix of particle masses such that

$$\boldsymbol{m} = \begin{bmatrix} m_1 & & & & \\ & \ddots & & & \\ & & m_i & & \\ & & & \ddots & \\ & & & & m_{N_p} \end{bmatrix} \in \mathbb{R}^{N_p \times N_p}. \tag{6}$$

Author Manuscript Author Manuscript Author Manuscript Author Manuscript

Splitting (5) yields two 1st-order ordinary differential equations,

$$\frac{d\boldsymbol{V}}{dt} = \boldsymbol{M}^{-1}\boldsymbol{F}(\boldsymbol{X}), \tag{7}$$

$$\frac{d\boldsymbol{X}}{dt} = \boldsymbol{V}, \tag{8}$$

where $\boldsymbol{V} = [\boldsymbol{v}_1^T, \ldots, \boldsymbol{v}_i^T, \ldots, \boldsymbol{v}_{N_p}^T]^T \in \mathbb{R}^{3N_p}$ and $\boldsymbol{v}_i$ is the velocity of particle, i. These equations are temporally discretized via Implicit Euler with a time step size of Δt. The unknown velocities and positions at time step, $n + 1$, as functions of the known values at time step, n, are given by

$$\boldsymbol{V}_{n+1} = \boldsymbol{V}_n + \Delta t \boldsymbol{M}^{-1}\boldsymbol{F}(\boldsymbol{X}_{n+1}), \tag{9}$$

$$\boldsymbol{X}_{n+1} = \boldsymbol{X}_n + \Delta t \boldsymbol{V}_{n+1}. \tag{10}$$

The forces are then separated into external and internal forces, such that $\boldsymbol{F}(\boldsymbol{X}_{n+1}) = \boldsymbol{F}_{ext} + \boldsymbol{F}_{int}(\boldsymbol{X}_{n+1})$. The external forces account for phenomena like gravity, while the internal forces arise from the constraints defining the mechanical behavior of the objects.

By combining (9) and (10), we obtain

$$\boldsymbol{M}\left(\boldsymbol{X}_{n+1} - 2\boldsymbol{X}_n + \boldsymbol{X}_{n-1} - \Delta t^2 \boldsymbol{M}^{-1}\boldsymbol{F}_{ext}\right) = \Delta t^2 \boldsymbol{F}_{int}(\boldsymbol{X}_{n+1}). \tag{11}$$

The goal of XPBD is to solve this linear system for $\boldsymbol{X}_{n+1}$. This is achieved via three sequential steps: 1) Prediction, 2) Constraint Projection, and 3) Update. The role of the Prediction step is to first obtain the initial particle positions that will be used in the Constraint Projection step. The Constraint Projection step then iteratively solves for these unknown positions. Finally, the Update step simply obtains the corrected velocities.

In the first step, XPBD estimates the value of $\boldsymbol{X}_{n+1}$ by accounting for inertial effects, which are induced by the particle velocities and the external forces. The velocities are updated first by evaluating

$$\boldsymbol{V}_{n+1} = \boldsymbol{V}_n + \Delta t \boldsymbol{M}^{-1}\boldsymbol{F}_{ext},$$

Author Manuscript Author Manuscript Author Manuscript Author Manuscript

(12)

and the estimated positions are then obtained by evaluating (10).

In the second step, the Constraint Projection step, XPBD iteratively corrects the positional estimates by using the internal forces, where the positions at the k^{th} iteration are $\boldsymbol{X}_{n+1}^{k}$. This update is performed separately for each constraint in the simulation, which has a total of N_c constraints. In the first iteration of this step, $\boldsymbol{X}_{n+1}^{k=1}$ is set to the value estimated from the Prediction step. The positional corrections for each subsequent iteration are then found by evaluating

$$\Delta \boldsymbol{X}_{n+1}^{k} = \Delta t^2 \boldsymbol{M}^{-1} \frac{\partial C_j(\boldsymbol{X})}{\partial \boldsymbol{X}}\bigg|_{\boldsymbol{x}_{n+1}^{k}} \Delta \lambda_{n+1,j}^{k}, \tag{13}$$

for each constraint in the simulation, where $\Delta \lambda_{n+1,j}^{k}$ defined as

$$\Delta \lambda_{n+1,j}^{k} = \frac{-C_j\left(\boldsymbol{X}_{n+1}^{k}\right) - \alpha_j \lambda_{n+1,j}^{k}}{\alpha_j + \Delta t^2 \left(\frac{\partial C_j(\boldsymbol{X})}{\partial \boldsymbol{X}}\right)^T\Big|_{\boldsymbol{x}_{n+1}^{k}} \boldsymbol{M}^{-1} \frac{\partial C_j(\boldsymbol{X})}{\partial \boldsymbol{X}}\Big|_{\boldsymbol{x}_{n+1}^{k}}}. \tag{14}$$

α_j is the inverse stiffness of the j^{th} constraint, C_j. We note that in our stenting simulator, C_j can be $C_{distance}$, $C_{bending}$, $C_{attachment}$, or $C_{collision}$. A derivation of (14) and (13) can be found in the supplementary material. $\lambda_{n+1,j}^{k}$ is an auxiliary variable that gets updated at each iteration via

$$\lambda_{n+1,j}^{k+1} = \lambda_{n+1,j}^{k} + \Delta \lambda_{n+1,j}^{k}, \tag{15}$$

Algorithm 1

Pseudocode for stenting simulation with XPBD

```
for n ∈ [1, N_t] do
    Inflate stent (increase radius)
    Perform Predict step for vessel particles:
        Estimate particle velocities with inertial effects via (12)
        Damp particle velocities (See Section 2.4)
        Estimate particle positions with inertial effects via (10)
    Detect collisions between vessel particles and stent SDF (See Section 2.4)
    Add vertex-normal collision constraints for vessel particles
    for k ∈ [1, N_i] do
        for j ∈ [1, N_c] do
            Perform Constraint Projection step for vessel particles:
```

Author Manuscript Author Manuscript Author Manuscript Author Manuscript

Obtain $\Delta\lambda^{k}_{n+1,j}$ via (14)
Obtain position corrections for particles via (13)
Update $\lambda^{k+1}_{n+1,j}$ via (15)
Update particle positions via (16)
end for
end for
Perform Update step for vessel particles:
Correct particle velocities via (17)
Remove vertex-normal collision constraints
end for

with $\lambda^{k=1}_{n+1,j}$ being initialized to 0. After solving for $\Delta \boldsymbol{X}^{k}_{n+1}$, we evaluate

$$\boldsymbol{X}^{k+1}_{n+1} = \boldsymbol{X}^{k}_{n+1} + \Delta \boldsymbol{X}^{k}_{n+1}, \tag{16}$$

to obtain the updated positions. This process is repeated for N_i iterations.

Finally, the Update step corrects the particle velocities estimated from the Prediction step by accounting for the contributions from the internal forces:

$$\boldsymbol{V}_{n+1} = \frac{\boldsymbol{X}_{n+1} - \boldsymbol{X}_{n}}{\Delta t}. \tag{17}$$

2.3 Stenting Simulator

Blood vessels and stents are modeled as distinct objects in our XPBD simulations. We model a blood vessel with a uniform, triangulated mesh and a stent with a signed distance field (SDF). Our stent modeling approach is detailed in Section 2.4. For each vertex on the vessel mesh, a corresponding particle is created for the simulation (Figure 2). As such, as the particles move during the simulation, the positions of the mesh vertices are updated, thereby deforming the mesh. The velocities are initialized to zero. Furthermore, we do not apply any external forces in our simulations.

We model the mechanical behavior of the vessel wall with distance constraints and bending constraints. One distance constraint is used per edge in the mesh and one bending constraint is created per pair of adjacent triangle elements (Figure 2). The deformations of the vessel are modeled through a one-way coupled interaction with the stent. Specifically, as the stent inflates and collides with the vessel, collision forces between the two objects are generated to deform the vessel.

To reduce the computational expense of our simulations, we clip the input vessel mesh to the region of interest—the stenosis and the immediate zone around the stenosis—using Paraview, a scientific visualization software [24], and perform the stenting simulations on

Author Manuscript Author Manuscript Author Manuscript Author Manuscript

this region. We fix the vertices lying on the boundaries of the clipped model to their original positions via attachment constraints to ensure that the entire mesh remains watertight as the clipped region deforms.

Our stenting technique is implemented in C++. We run the XPBD simulation for N_t time steps to incrementally inflate the stent and expand the stenosis. Our method is summarized in Algorithm 1. The deformed model at the final time step represents the lumen of the stented vessel. We illustrate our stenting technique on two idealized blood vessels in Figure 4.

2.4 Stent Modeling and Collisions

We specify the deformations of the stent kinematically. This is achieved by simply incrementally increasing the radius, R, of the stent at the beginning of each time step. We also represent the stent by the zero level set of an SDF of a curved, capped cylinder. However, the SDF of a capped cylinder with arbitrarily varying curvature along its centerline cannot be computed analytically. As such, we instead approximate this SDF, $\phi(\boldsymbol{x}, R)$, by taking the union of multiple SDFs corresponding to shorter, straight cylinders (Figure 3). The union of multiple SDFs can simply be computed as their minimum signed distance.

The centerline, $\mathscr{L}$, of the curved cylinder is represented by a discrete set of N_L ordered points, such that $\mathscr{L} = \{\boldsymbol{x}_1, \ldots, \boldsymbol{x}_m, \ldots, \boldsymbol{x}_{N_L}\}$. The equation for the SDF is thus given by

$$\phi(\boldsymbol{x}, R) = \min\left(\mathscr{C}(\boldsymbol{x}, \boldsymbol{x}_1, \boldsymbol{x}_2, R), \ldots, \mathscr{C}(\boldsymbol{x}, \boldsymbol{x}_m, \boldsymbol{x}_{m+1}, R), \ldots, \mathscr{C}(\boldsymbol{x}, \boldsymbol{x}_{N_L-1}, \boldsymbol{x}_{N_L}, R)\right), \tag{18}$$

where $\mathscr{C}(\boldsymbol{x}, \boldsymbol{x}_m, \boldsymbol{x}_{m+1}, R)$ is the signed distance at any point, $\boldsymbol{x}$, with respect to a straight cylinder of radius, R, with cap centroids at $\boldsymbol{x}_m$ and $\boldsymbol{x}_{m+1}$.

We set the centerline of the curved stent in its initial state to coincide with the centerline of the vessel the stent is embedded in. To generate the centerlines of the vessel surface meshes, we use the centerline extraction tool in the Vascular Modeling Toolkit [25] and SimVascular [26]. If we maintain this centerline throughout the entire XPBD simulation, then the deployed stent will conform to the native curvature of the vessel. This behavior is characteristic of open-cell stents (Figure 4) [27]. However, we can also straighten the stent by incrementally displacing the centerline points until their final arrangement corresponds to the centerline of a straight cylinder. This allows the inflating stent to also straighten curved vessels, which is similar to the behavior of closed-cell stents.

We detect collisions between the stent SDF and the vessel mesh by using the signed distance of each mesh particle. If the signed distance meets the threshold value, we add a corresponding vertex-normal constraint to our simulator. Specifically, $(\boldsymbol{x} - \boldsymbol{x}_c) \cdot \boldsymbol{n}_c$ in (3) is set as the signed distance value of the particle and d_c is set as the threshold value.

To reduce jittering artifacts from collision responses or other internal forces in our simulations, we damp the velocity obtained from (12) for each particle [21]. Various

Author Manuscript Author Manuscript Author Manuscript Author Manuscript

methods have been developed for damping in XPBD [23]. We choose a simple damping technique that caps the particle velocity magnitude to a maximum value of $\frac{\xi d_c}{\Delta t}$, where ξ is a damping constant.

2.5 Computational Fluid Dynamics Simulations

After completing the XPBD simulation, we can prepare the stented model for CFD analysis. To do this, we first remesh the stented vessel surface mesh and perform Laplacian smoothing in the clipped region. These steps can be easily performed with the remeshing and smoothing functionalities in SimVascular (https://github.com/SimVascular/SimVascular), an open-source framework for cardiovascular modeling [28]. Afterwards, we generate the volume mesh and apply boundary conditions. In the following results, we conduct CFD simulations with svSolver (https://github.com/SimVascular/svSolver), a free software for numerically solving the Navier-Stokes equations with a stabilized finite element method. svSolver uses linear tetrahedral shape functions for spatial discretization and the generalized-α method for time discretization [29, 30]. The discretized system is solved with a custom linear solver and preconditioner [31]. We perform rigid wall simulations [32]; however, deformable wall simulations via fluid-structure interaction can be simulated as well [33].

3 Results and Discussion

We demonstrate the application of our virtual stenting method in this section. All preoperative models used here were obtained from the Vascular Model Repository (https://www.vascularmodel.com/) [34], an open-source collection of patient-specific cardiovascular models created with SimVascular. The results presented in this section were generated with stiffness values of 10^5, 10^3, and 10^5 for the distance, bending, and vertex-normal collision constraints, respectively.

3.1 Patient-Specific Stenting

We first illustrate our stenting method on a patient-specific pulmonary artery in Figure 1. Observe that our technique can edit the shape of the input vessel to create a stented configuration without creating erroneous artifacts in the mesh. This is in contrast to the stented model generated via segmentation editing. Furthermore, only a minimal prescription of the stented shape was required with our technique. The shape was automatically determined from the vessel centerline and a given target stent diameter in the XPBD simulation. In the segmentation-editing case, the contours corresponding to the stented lumen were manually scripted.

To demonstrate the generalizability of our method, we also created stenting shape edits on six additional patient-specific meshes in Figure 5. These models span a wide range of vascular anatomies and diseases. The top row of this figure shows stenting of three aortic models corresponding to patients with coarctation of the aorta. To relieve the constrictions, the meshes were inflated until the diameter of the stent matched the minimum lumen cross-sectional area proximal and distal to the stenosis. For these models, we maintained

Author Manuscript Author Manuscript Author Manuscript Author Manuscript

the original centerline throughout the simulations. This allowed the stents to conform to the native aortic curvature.

The second row illustrates stenting in an aortofemoral network with aortoiliac occlusive disease. We see full restoration of the lumen area at the lesion site here. The last two rows demonstrate stenting in two patient-specific pulmonary models with diffuse stenoses throughout the left and right pulmonary arteries. Stenting was performed in the proximal regions of both arteries near the junction regions. These models correspond to patients with Alagille and Williams Syndromes, respectively. We based these examples on the studies conducted by Lan et al. [11]. In the Williams model, we straightened the stent dynamically by modifying the stent centerline points, as discussed in Section 2.4, to represent closed-cell stenting [35]. This can be observed in the boxed region, in which the vessel changes its curvature from the preoperative shape to the postoperative shape. We maintained the native curvature in the Alagille model.

3.2 Hemodynamic Simulations

Our methods can also be coupled to CFD simulations to systematically assess the efficacy of stenting procedures. We demonstrate an example application in Figure 6. In this figure, we virtually inflated a patient-specific aortic coarctation with various stent diameters and simulated the resulting aortic pressure. The CFD simulations were performed using an unsteady inflow boundary condition with a parabolic profile at the inlet cap and three-element Windkessel boundary conditions [36] at the outlet caps [37]. Parameter values for these boundary conditions can be found in the Vascular Model Repository (model 0069 0001). Based on a mesh convergence study, we used meshes with approximately 1.6 million linear tetrahedral elements to achieve a relative error tolerance of 3% for our measurements of the pressure gradient across the stenosis. We observe significant gradients in mean pressure across the stenosis in the first three cases. This pressure gradient reduces as the stent is inflated to a larger size.

This example highlights a “digital twin” application of our method in which clinicians can investigate the potential impact of their intended intervention on a virtual model before performing the procedure in the clinic. Simulated hemodynamics can be used to determine the degree of stent inflation needed to achieve a target pressure outcome. This capability will help clinicians develop outcome-driven treatment plans, which will ultimately help mitigate potential risks, such as in-stent restenosis [6, 38].

3.3 Synthetic Data Generation

In Figure 7, we demonstrate an application of synthetic data generation with our method. To create the models, we first applied recently developed Kelvinlet-based techniques [15] to induce artificial stenoses at various locations on a healthy patient-specific coronary model. Afterwards, we relieved the lesions with our virtual stenting technique and simulated the resulting hemodynamics for each model. CFD simulations were performed on meshes with approximately 3.5 million tetrahedral elements. An unsteady inflow boundary condition with a Womersley profile at the aortic inlet, along with a Windkessel boundary condition at the aortic outlet and coronary boundary conditions at the coronary outlets [39], were used. The

Author Manuscript Author Manuscript Author Manuscript Author Manuscript

exact parameter values for these boundary conditions can be found in the Vascular Model Repository (model 0186 0002). As expected, the diseased models demonstrate significant pressure drops across the coronary stenoses, while the stented models have similar pressure distributions to the healthy case.

Generating synthetic data, as in this example, is essential for data-driven modeling techniques. Pure physics-based CFD simulations are computationally expensive, with single simulations on a high-performance supercomputer requiring hours to days to complete. However, real-time hemodynamic simulations are increasingly possible, thanks to recent progress in machine learning, including physics-informed machine learning methods [40]. The proposed stenting method, along with Kelvinlets, can be used to create large ensembles of synthetic models that represent realistic preoperative and postoperative stenting procedures. This data can then be used to train machine-learning frameworks that enable fast hemodynamic predictions of stenting outcomes [41]. Such developments are essential for creating realistic scenarios in virtual reality for medical training [42] and helping clinicians rapidly make hemodynamically informed decisions for emergency operations.

Additionally, by coupling our method with techniques for geometric uncertainty quantification, future studies could parametrically generate stented models with slight geometric variations that reflect uncertainties in the final stent diameter, length, and position. These geometric variations can be achieved by altering the prescribed stent diameter and chosen centerline points. These models can then be used to create corresponding confidence intervals in the estimated hemodynamic values [43]. Providing these statistics to clinicians will help them better assess potential risks for their patients.

3.4 Limitations and Future Work

We have developed a method based on XPBD simulations to guide the shape-editing process and create plausible shapes of stented vessels. Two interventional cardiologists with extensive experience qualitatively confirmed the post-intervention appearance to be clinically feasible, reasonable, and in line with what they would expect given their experience. We highlight that the primary goal of this XPBD-based work is to provide an efficient means to explore a wide range of potential stenting scenarios to support treatment planning efforts. This will also be useful for selecting a small number of promising scenarios to perform expensive high-fidelity, full physics simulations in future work. Nevertheless, to further ensure the clinical realism of our XPBD approach in future work, we plan to quantitatively compare the shapes and resulting bulk hemodynamics of vessels stented using our XPBD-based approach against patient-specific stenting procedures. To perform these validation studies, pre- and post-intervention images of vessels from a range of patient-specific cases of cardiovascular diseases are needed. We will work with clinicians to obtain such data.

We leverage XPBD to provide an effective alternative to produce a range of realistic stented vessel geometries to guide clinical decision-making, as opposed to applying expensive numerical simulations to make predictions of treatment outcomes. Such outcome predictions are generally performed by instead simulating the full physics underlying

Author Manuscript Author Manuscript Author Manuscript Author Manuscript

stenting procedures with traditional techniques, such as the finite element method (FEM). However, one advantage of FEM-based approaches compared to our XPBD-based approach is that FEM simulations allow one to quantify the stresses induced by the stent on the vessel wall and vice versa [44, 45]. This could help characterize the potential for vascular injury and in-stent restenosis via growth and remodeling processes [46]. Despite these advantages, FEM simulations are generally computationally expensive, requiring compute times of hours to days, even on multiprocessor supercomputers, compared to XPBD-based simulations, which have compute times on the order of minutes for a single processor in a standard workstation. In follow-up work, we plan to perform quantitative comparisons of our XPBD-generated models with those produced by FEM simulations. Towards this goal, hyperelastic constitutive laws representing the mechanics of vascular tissues are needed [44]. The material properties of diseased vessels must specifically be accounted for, as these tissues generally have different microstructural constituents from their healthy equivalents [47]. We note that XPBD could also be used as a fast technique for exploring potential clinical scenarios prior to performing a full-physics FEM simulation in future work.

Our technique assumes that the centerline of the stent coincides with the centerline of the vessel lumen. This assumption works well for performing stenting of stenoses that are concentric with the vessel wall [48]. However, for an off-centered stenosis, which is located radially closer to one side of the vessel wall, this assumption would cause that side to over-expand during the deformation process as the stent inflates. We will explore approaches in stent centerline prescription and vessel centerline deformation to overcome this limitation and perform stenting of nonconcentric stenoses in future work.

The proposed method models the bulk, global cylindrical-like shape of stents. This is useful for CFD analyses that aim to simulate changes in bulk hemodynamic quantities, such as average pressures. Such predictions are needed in many clinical applications, for example in determining if a pulmonary artery stenting scenario has adequately reduced right ventricular pressure [11]. Our technique, however, does not model the detailed strut structures of the stent and their effects on local vessel hemodynamics, such as wall shear stress [49]. One approach to model these finer geometric characteristics would be to use an SDF that represents the actual wire mesh of the stent; this is an avenue for future work.

Another limitation of our method is that it does not account for self-collisions in the vessel mesh. We have not found this to be an issue in our examples. However, in situations where stenting a vessel branch may cause it to collide with a nearby branch, simulating such self-collisional events is essential. Additional collision constraints are needed to resolve such behavior [22]. The collisions between these mesh facets can be detected using spatial hashing or other collision detection techniques [50].

Our method also does not yet model two-way coupled interactions between vessels and stents. The stents are modeled such that they can deform the vessels they are embedded in, but the vessels cannot deform the stents. In clinical stenting operations, the stents can, however, deform during and after deployment from interactions with vessels and/or surrounding tissue and structures. Additional work is needed to simulate such coupled behavior. In particular, the stent must be represented as a mesh, with additional constraints

Author Manuscript Author Manuscript Author Manuscript Author Manuscript

modeling the mechanical behavior of the stent. Collision constraints between the facets on the stent and the vessel meshes would be required as well. We will explore these extensions in future work.

The proposed method could also be used to perform shape edits that mimic other interventional and surgical procedures. Particular operations of interest could include graft attachment for the Fontan operation and patch augmentation for reconstructive surgeries. To enable these operations, mesh-cutting techniques, leveraging existing ideas from literature [51], could be coupled with our XPBD-based methods. Finally, we plan to make our stenting method and subsequent developments available open-source in the future, as part of the larger SimVascular ecosystem.

4 Conclusions

We have developed a novel shape-editing method to virtually stent patient-specific blood vessels using simulated mesh deformations. To perform shape edits, we place a stent inside the lumen of a vessel and deform the vessel mesh with XPBD simulations as the stent inflates and collides with the vessel wall. Our method works across a large range of vascular anatomies, including the aorta, coronary arteries, pulmonary tree, and femoral vessels. With the proposed method, one can also parametrically generate plausible geometric variations in the stented configuration. This functionality will enable the creation of large ensembles of models to support data-driven applications, such as machine learning and uncertainty quantification. Additionally, clinicians could use the proposed methods to noninvasively predict the hemodynamic impacts of an intended stent-based intervention on a digital twin of their patient as part of the complex decision and treatment planning process. This will aid enable clinicians to better weigh the potential benefits and risks of a treatment. Future studies will investigate advancements to model the stent as a deformable entity and perform shape edits representing surgical operations, such as grafting.

Supplementary Material

Refer to Web version on PubMed Central for supplementary material.

Acknowledgements.

The authors thank Dr. Doff McElhinney, Zachary Sexton, Weiguang Yang, Karthik Menon, and the Cardiovascular Biomechanics Computation Lab at Stanford University for technical discussions and support on this work.

Funding.

This work was supported by NIH grants R01EB029362, R01LM013120, R01HL141712, and R01HL167516 and NSF grants 1663671 and 2105345.

References

[1]. Tsao CW, Aday AW, Almarzooq ZI, Anderson CAM, Arora P, Avery CL, Baker-Smith CM, Beaton AZ, Boehme AK, Buxton AE, Commodore-Mensah Y, Elkind MSV, Evenson KR, Eze-Nliam C, Fugar S, Generoso G, Heard DG, Hiremath S, Ho JE, Kalani R, Kazi DS, Ko D, Levine DA, Liu J, Ma J, Magnani JW, Michos ED, Mussolino ME, Navaneethan SD, Parikh NI, Poudel R, Rezk-Hanna M, Roth GA, Shah NS, St-Onge M-P, Thacker EL, Virani SS, Voeks

Author Manuscript Author Manuscript Author Manuscript Author Manuscript

JH, Wang N-Y, Wong ND, Wong SS, Yaffe K, Martin SS, null: Heart disease and stroke statistics —2023 update: A report from the american heart association. Circulation 147(8), 93–621 (2023) 10.1161/CIR.0000000000001123

[2]. Geggel RL, Gauvreau K, Lock JE: Balloon dilation angioplasty of peripheral pulmonary stenosis associated with williams syndrome. Circulation 103(17), 2165–2170 (2001) 10.1161/01.CIR.103.17.2165 [PubMed: 11331257]

[3]. Pijls NHJ, Klauss V, Siebert U, Powers E, Takazawa K, Fearon WF, Escaned J, Tsurumi Y, Akasaka T, Samady H, Bruyne BD: Coronary pressure measurement after stenting predicts adverse events at follow-up. Circulation 105(25), 2950–2954 (2002) 10.1161/01.CIR.0000020547.92091.76 [PubMed: 12081986]

[4]. Mitra AK, Agrawal DK: In stent restenosis: bane of the stent era. J Clin Pathol 59(3), 232–239 (2006) [PubMed: 16505271]

[5]. Kim MS, Dean LS: In-stent restenosis. Cardiovascular Therapeutics 29(3), 190–198 (2011) 10.1111/j.1755-5922.2010.00155.x [PubMed: 20406239]

[6]. Ng J, Bourantas CV, Torii R, Ang HY, Tenekecioglu E, Serruys PW, Foin N: Local hemodynamic forces after stenting: Implications on restenosis and thrombosis. Arteriosclerosis, Thrombosis, and Vascular Biology 37(12), 2231–2242 (2017) 10.1161/ATVBAHA.117.309728 [PubMed: 29122816]

[7]. Taylor CA, Figueroa CA: Patient-specific modeling of cardiovascular mechanics. Annual Review of Biomedical Engineering 11(1), 109–134 (2009) 10.1146/annurev.bioeng.10.061807.160521 PMID: 19400706

[8]. Gray RA, Pathmanathan P: Patient-specific cardiovascular computational modeling: Diversity of personalization and challenges. Journal of Cardiovascular Translational Research 11(2), 80–88 (2018) 10.1007/s12265-018-9792-2 [PubMed: 29512059]

[9]. Hachem E, Meliga P, Goetz A, Rico PJ, Viquerat J, Larcher A, Valette R, Sanches AF, Lannelongue V, Ghraieb H, Nemer R, Ozpeynirci Y, Liebig T: Reinforcement learning for patient-specific optimal stenting of intracranial aneurysms. Scientific Reports 13(1), 7147 (2023) 10.1038/s41598-023-34007-z [PubMed: 37130900]

[10]. Morris PD, Narracott A, Tengg-Kobligk H, Soto DAS, Hsiao S, Lungu A, Evans P, Bressloff NW, Lawford PV, Hose DR, Gunn JP: Computational fluid dynamics modelling in cardiovascular medicine. Heart 102(1), 18–28 (2016) 10.1136/heartjnl-2015-308044 [PubMed: 26512019]

[11]. Lan IS, Yang W, Feinstein JA, Kreutzer J, Collins RT, Ma M, Adamson GT, Marsden AL: Virtual transcatheter interventions for peripheral pulmonary artery stenosis in williams and alagille syndromes. Journal of the American Heart Association 11(6), 023532 (2022) 10.1161/JAHA.121.023532

[12]. Luffel M, Sati M, Rossignac J, Yoganathan AP, Haggerty CM, Restrepo M, Slesnick TC, Kanter KR, del Nido P, Fogel MA: Surgem: A solid modeling tool for planning and optimizing pediatric heart surgeries. Computer-Aided Design 70, 3–12 (2016) 10.1016/j.cad.2015.06.018. SPM 2015

[13]. Kjeldsberg HA, Bergersen AW, Valen-Sendstad K: morphMan: Automated manipulation of vascular geometries. Journal of Open Source Software 4(35), 1065 (2019) 10.21105/joss.01065

[14]. Pham J, Wyetzner S, Pfaller MR, Parker DW, James DL, Marsden AL: svMorph: Interactive Geometry-Editing Tools for Virtual Patient-Specific Vascular Anatomies. Journal of Biomechanical Engineering 145(3) (2022) 10.1115/1. 4056055 https://asmedigitalcollection.asme.org/biomechanical/article-pdf/145/3/031001/6954064/bio_145_03_031001.pdf. 031001

[15]. Pham J, Kong F, James DL, Marsden AL: Virtual shape-editing of patient-specific vascular models using Regularized Kelvinlets. IEEE Transactions on Biomedical Engineering, 1–14 (2024) 10.1109/TBME.2024.3355307

[16]. Shi H, Ames J, Randles A: Harvis: An interactive virtual reality tool for hemodynamic modification and simulation. Journal of Computational Science 43, 101091 (2020) 10.1016/j.jocs.2020.101091

[17]. Macklin M, Müller M, Chentanez N: XPBD: Position-based simulation of compliant constrained dynamics. In: Proceedings of the 9th International Conference on Motion in Games.

Author Manuscript Author Manuscript Author Manuscript Author Manuscript

MIG '16, pp. 49–54. Association for Computing Machinery, New York, NY, USA (2016). 10.1145/2994258.2994272.

[18]. Segato A, Vece CD, Zucchelli S, Marzo MD, Wendler T, Azampour MF, Galvan S, Secoli R, De Momi E: Position-based dynamics simulator of brain deformations for path planning and intra-operative control in keyhole neurosurgery. IEEE Robotics and Automation Letters 6(3), 6061–6067 (2021) 10.1109/LRA.2021.3090016

[19]. Walczak L, Georgii J, Tautz L, Neugebauer M, Wamala I, Sündermann S, Falk V, Hennemuth A: Using position-based dynamics for simulating mitral valve closure and repair procedures. Computer Graphics Forum 41(1), 270–287 (2022) 10.1111/cgf.14434

[20]. Witkin A, Baraff D: Physically based modeling: Principles and practice. (1997). http://www.cs.cmu.edu/~baraff/sigcourse/

[21]. Baraff D, Witkin A: Large steps in cloth simulation. In: Proceedings of the 25th Annual Conference on Computer Graphics and Interactive Techniques. SIGGRAPH '98, pp. 43–54. Association for Computing Machinery, New York, NY, USA (1998). 10.1145/280814.280821.

[22]. Müller M, Heidelberger B, Hennix M, Ratcliff J: Position based dynamics. Journal of Visual Communication and Image Representation 18(2), 109–118 (2007) 10.1016/j.jvcir.2007.01.005

[23]. Bender J, Müller M, Macklin M: A survey on position based dynamics, 2017. In: Proceedings of the European Association for Computer Graphics: Tutorials. EG '17. Eurographics Association, Goslar, DEU (2017). 10.2312/egt.20171034.

[24]. Ayachit U: The ParaView Guide: A Parallel Visualization Application. Kitware, Inc., Clifton Park, NY, USA (2015)

[25]. Izzo R, Steinman D, Manini S, Antiga L: The vascular modeling toolkit: A python library for the analysis of tubular structures in medical images. Journal of Open Source Software 3(25), 745 (2018) 10.21105/joss.00745

[26]. Pfaller MR, Pham J, Verma A, Pegolotti L, Wilson NM, Parker DW, Yang W, Marsden AL: Automated generation of 0d and 1d reduced-order models of patient-specific blood flow. International Journal for Numerical Methods in Biomedical Engineering 38(10), 3639 (2022) 10.1002/cnm.3639

[27]. Pierce DS, Rosero EB, Modrall JG, Adams-Huet B, Valentine RJ, Clagett GP, Timaran CH: Open-cell versus closed-cell stent design differences in blood flow velocities after carotid stenting. Journal of Vascular Surgery 49(3), 602–606 (2009) 10.1016/j.jvs.2008.10.016 [PubMed: 19268763]

[28]. Updegrove A, Wilson NM, Merkow J, Lan H, Marsden AL, Shadden SC: Simvascular: An open source pipeline for cardiovascular simulation. Annals of Biomedical Engineering 45(3), 525–541 (2017) 10.1007/s10439-016-1762-8 [PubMed: 27933407]

[29]. Franca LP, Frey SL: Stabilized finite element methods: Ii. the incompressible Navier-Stokes equations. Computer Methods in Applied Mechanics and Engineering 99(2), 209–233 (1992) 10.1016/0045-7825(92)90041-H

[30]. Whiting CH, Jansen KE: A stabilized finite element method for the incompressible Navier–Stokes equations using a hierarchical basis. International Journal for Numerical Methods in Fluids 35(1), 93–116 (2001) 10.1002/1097-0363(20010115)35:1⟨93::AID-FLD85⟩3.0.CO;2-G

[31]. Esmaily-Moghadam M, Bazilevs Y, Marsden AL: A new preconditioning technique for implicitly coupled multidomain simulations with applications to hemodynamics. Computational Mechanics 52(5), 1141–1152 (2013) 10.1007/s00466-013-0868-1

[32]. Taylor CA, Hughes TJR, Zarins CK: Finite element modeling of blood flow in arteries. Computer Methods in Applied Mechanics and Engineering 158(1), 155–196 (1998) 10.1016/S0045-7825(98)80008-X

[33]. Figueroa CA, Vignon-Clementel IE, Jansen KE, Hughes TJR, Taylor CA: A coupled momentum method for modeling blood flow in three-dimensional deformable arteries. Computer Methods in Applied Mechanics and Engineering 195(41), 5685–5706 (2006) 10.1016/j.cma.2005.11.011. John H. Argyris Memorial Issue. Part II

[34]. Wilson NM, Ortiz AK, Johnson AB: The Vascular Model Repository: A Public Resource of Medical Imaging Data and Blood Flow Simulation Results. Journal of Medical Devices

Author Manuscript Author Manuscript Author Manuscript Author Manuscript

7(4) (2013) 10.1115/1.4025983 https://asmedigitalcollection.asme.org/medicaldevices/article-pdf/7/4/040923/6234847/med_007_04_040923.pdf. 040923

[35]. Travelli FC, Sullivan PM, Takao C, Ing FF: The valeo stent: a premounted, open-cell, large stent for use in small children with chd. Cardiology in the Young 26(6), 1187–1193 (2016) 10.1017/S104795111500219X [PubMed: 26593884]

[36]. Vignon-Clementel IE, Figueroa KEJCA, Taylor CA: Outflow boundary conditions for 3d simulations of non-periodic blood flow and pressure fields in deformable arteries. Computer Methods in Biomechanics and Biomedical Engineering 13(5), 625–640 (2010) 10.1080/10255840903413565 . [PubMed: 20140798]

[37]. Menon A, Wendell DC, Wang H, Eddinger TJ, Toth JM, Dholakia RJ, Larsen PM, Jensen ES, LaDisa JF: A coupled experimental and computational approach to quantify deleterious hemodynamics, vascular alterations, and mechanisms of long-term morbidity in response to aortic coarctation. Journal of Pharmacological and Toxicological Methods 65(1), 18–28 (2012) 10.1016/j.vascn.2011.10.003 [PubMed: 22079597]

[38]. Colombo M, He Y, Corti A, Gallo D, Ninno F, Casarin S, Rozowsky JM, Migliavacca F, Berceli S, Chiastra C: In-stent restenosis progression in human superficial femoral arteries: Dynamics of lumen remodeling and impact of local hemodynamics. Annals of Biomedical Engineering 49(9), 2349–2364 (2021) 10.1007/s10439-021-02776-1 [PubMed: 33928465]

[39]. Kim HJ, Vignon-Clementel IE, Coogan JS, Figueroa CA, Jansen KE, Taylor CA: Patient-specific modeling of blood flow and pressure in human coronary arteries. Annals of Biomedical Engineering 38(10), 3195–3209 (2010) 10.1007/s10439-010-0083-6 [PubMed: 20559732]

[40]. Karniadakis GE, Kevrekidis IG, Lu L, Perdikaris P, Wang S, Yang L: Physics-informed machine learning. Nature Reviews Physics 3(6), 422–440 (2021) 10.1038/s42254-021-00314-5

[41]. Lee JD, Richter J, Pfaller MR, Szafron JM, Menon K, Zanoni A, Ma MR, Feinstein JA, Kreutzer J, Marsden AL, Schiavazzi DE: A Probabilistic Neural Twin for Treatment Planning in Peripheral Pulmonary Artery Stenosis (2023)

[42]. Gallagher AG, Cates CU: Approval of Virtual Reality Training for Carotid Stenting: What This Means for Procedural-Based Medicine. JAMA 292(24), 3024–3026 (2004) 10.1001/jama.292.24.3024 [PubMed: 15613672]

[43]. Maher GD, Fleeter CM, Schiavazzi DE, Marsden AL: Geometric uncertainty in patient-specific cardiovascular modeling with convolutional dropout networks. Computer Methods in Applied Mechanics and Engineering 386, 114038 (2021) 10.1016/j.cma.2021.114038 [PubMed: 34737480]

[44]. Lally C, Dolan F, Prendergast PJ: Cardiovascular stent design and vessel stresses: A finite element analysis. Journal of Biomechanics 38(8), 1574–1581 (2005) 10.1016/j.jbiomech.2004.07.022 [PubMed: 15958213]

[45]. Migliavacca F, Petrini L, Colombo M, Auricchio F, Pietrabissa R: Mechanical behavior of coronary stents investigated through the finite element method. Journal of Biomechanics 35(6), 803–811 (2002) 10.1016/S0021-9290(02)00033-7 [PubMed: 12021000]

[46]. Zahedmanesh H, Lally C: Determination of the influence of stent strut thickness using the finite element method: implications for vascular injury and in-stent restenosis. Medical & Biological Engineering & Computing 47(4), 385–393 (2009) 10.1007/s11517-009-0432-5 [PubMed: 19189146]

[47]. Chen H, Kassab GS: Microstructure-based biomechanics of coronary arteries in health and disease. Journal of Biomechanics 49(12), 2548–2559 (2016) 10.1016/j.jbiomech.2016.03.023. Cardiovascular Biomechanics in Health and Disease [PubMed: 27086118]

[48]. Dodds SR: The haemodynamics of asymmetric stenoses. European Journal of Vascular and Endovascular Surgery 24(4), 332–337 (2002) 10.1053/ejvs.2002.1729 [PubMed: 12323176]

[49]. LaDisa JF, Guler I, Olson LE, Hettrick DA, Kersten JR, Warltier DC, Pagel PS: Three-dimensional computational fluid dynamics modeling of alterations in coronary wall shear stress produced by stent implantation. Annals of Biomedical Engineering 31(8), 972–980 (2003) 10.1114/1.1588654 [PubMed: 12918912]

Author Manuscript Author Manuscript Author Manuscript Author Manuscript

[50]. Teschner M, Kimmerle S, Heidelberger B, Zachmann G, Raghupathi L, Fuhrmann A, Cani M-P, Faure F, Magnenat-Thalmann N, Strasser W, Volino P: Collision detection for deformable objects. Computer Graphics Forum 24(1), 61–81 (2005) 10.1111/j.1467-8659.2005.00829.x

[51]. Berndt I, Torchelsen R, Maciel A: Efficient surgical cutting with position-based dynamics. IEEE Computer Graphics and Applications 37(3), 24–31 (2017) 10.1109/MCG.2017.45 [PubMed: 28459669]

Author Manuscript Author Manuscript Author Manuscript Author Manuscript

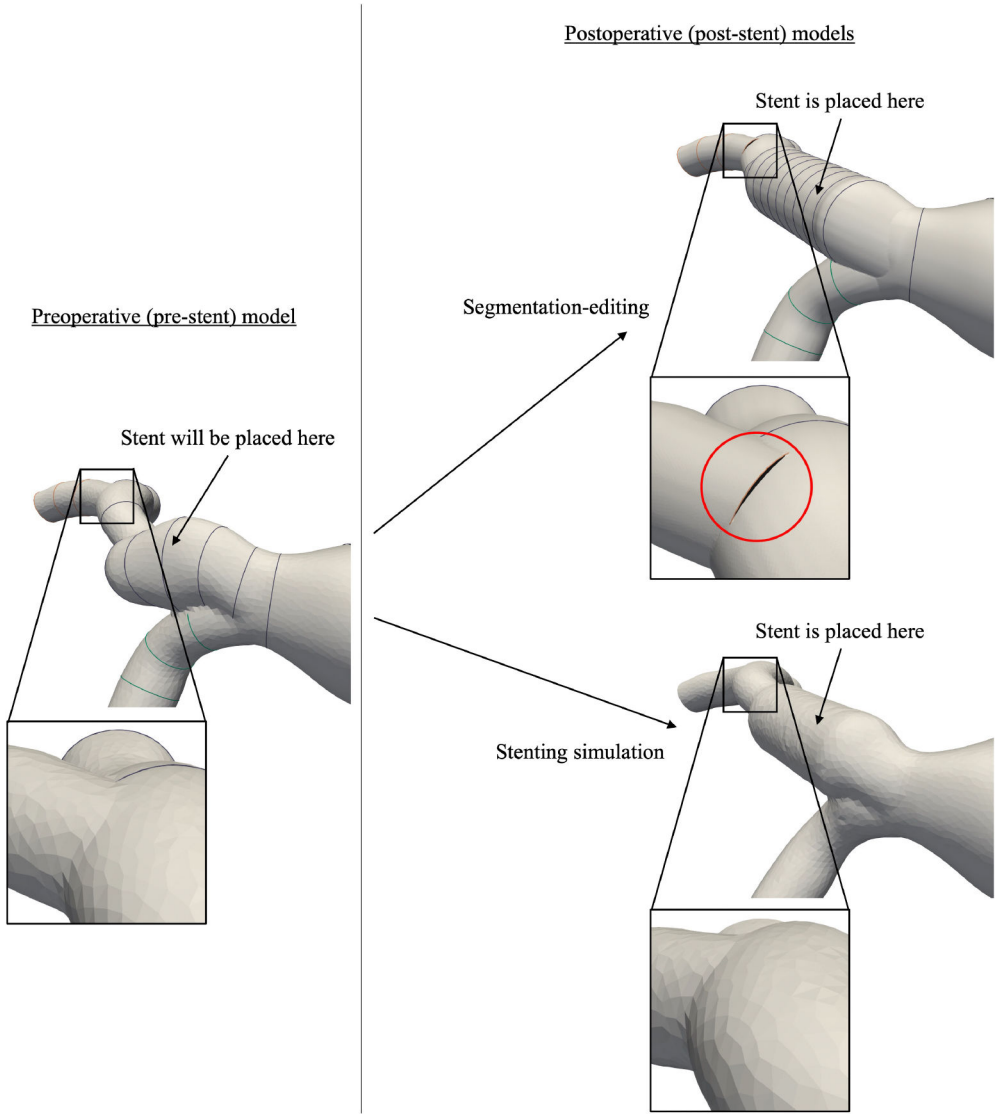

Fig. 1.

Postoperative, stented models of a pulmonary network were created from a preoperative model (left) via two methods: 1) script-based segmentation editing (top right) and 2) XPBD simulations (bottom right). The final contours of the stented model in the segmentation-editing case did not yield a proper loft, resulting in an artificial cap face (circled in red in the top right inset) in the stented model. Our simulation-guided technique, which does not involve any segmentation editing, does not produce such artifacts.

Author Manuscript Author Manuscript Author Manuscript Author Manuscript

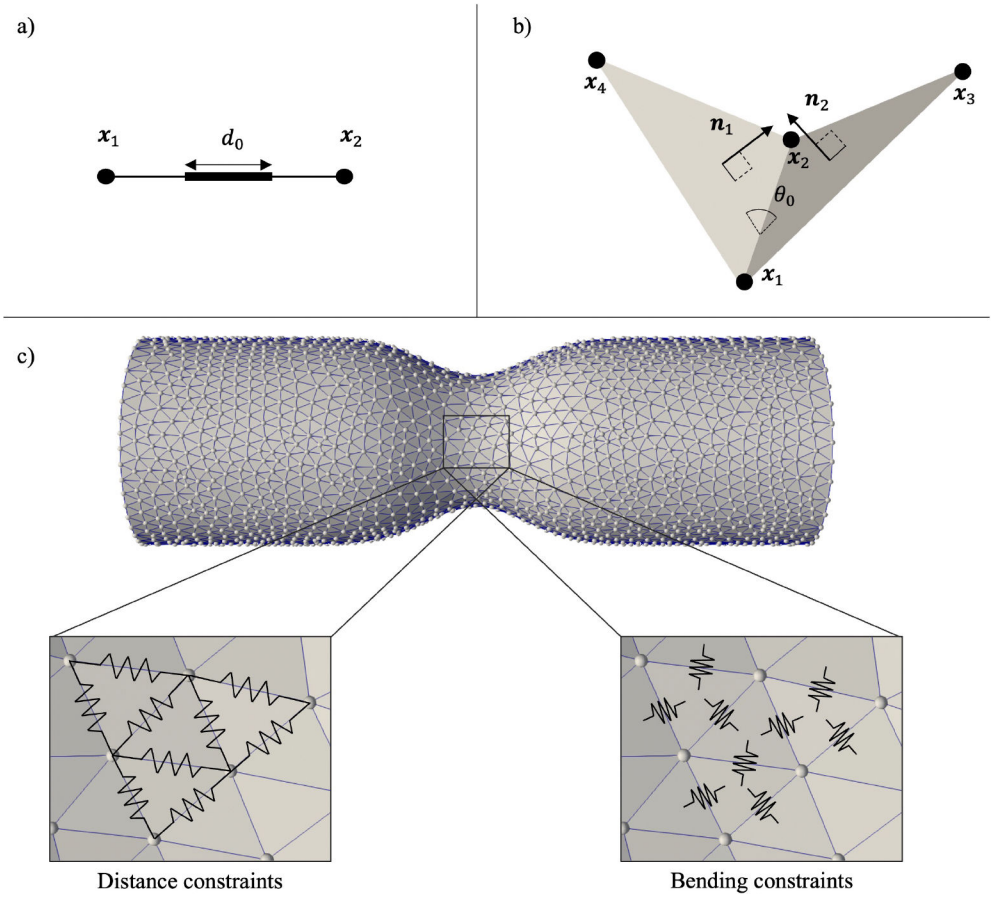

Fig. 2.

a) The distance constraint aims to restore the distance between two particles, $\boldsymbol{x}_1$ and $\boldsymbol{x}_2$, to the rest distance, d_0. b) The bending constraint aims to restore the angle between the first triangle cell (with particles, $\boldsymbol{x}_1$, $\boldsymbol{x}_2$, $\boldsymbol{x}_4$ and unit normal vector, $\boldsymbol{n}_1$) and the second triangle cell (with particles, $\boldsymbol{x}_1$, $\boldsymbol{x}_2$, $\boldsymbol{x}_3$ and unit normal vector, $\boldsymbol{n}_2$) to the rest angle, θ_0. c) In the vessel mesh, one particle is created for each vertex for the XPBD simulation. Furthermore, there is one distance constraint (visualized as a spring) for each edge in the mesh and one bending constraint (also visualized as a spring) for each pair of neighboring triangle elements.

Author Manuscript Author Manuscript Author Manuscript Author Manuscript

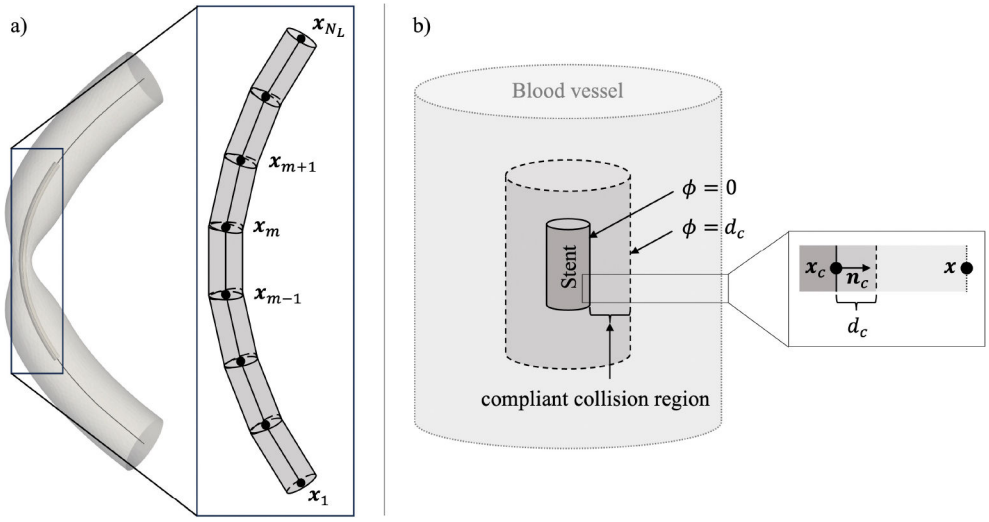

Fig. 3.

a) The SDF for a curved, capped cylinder with an arbitrary centerline of N_L points is approximated as the union of multiple SDFs of shorter, straight capped cylinders. b) Collisions between a stent, represented by the zero level set of the SDF, ϕ, and particles on a deformable vessel mesh are detected when the signed distance between the particles and the stent is less than the threshold distance, d_c. Vertex-normal collision constraints are used as the corresponding collision responses. These constraints aim to restore the distance between a particle, $\boldsymbol{x}$, on the mesh and the collision point, $\boldsymbol{x}_c$, on the stent to the threshold distance, d_c, where $\boldsymbol{n}_c$ is the unit normal vector of the stent at $\boldsymbol{x}_c$.

Author Manuscript Author Manuscript Author Manuscript Author Manuscript

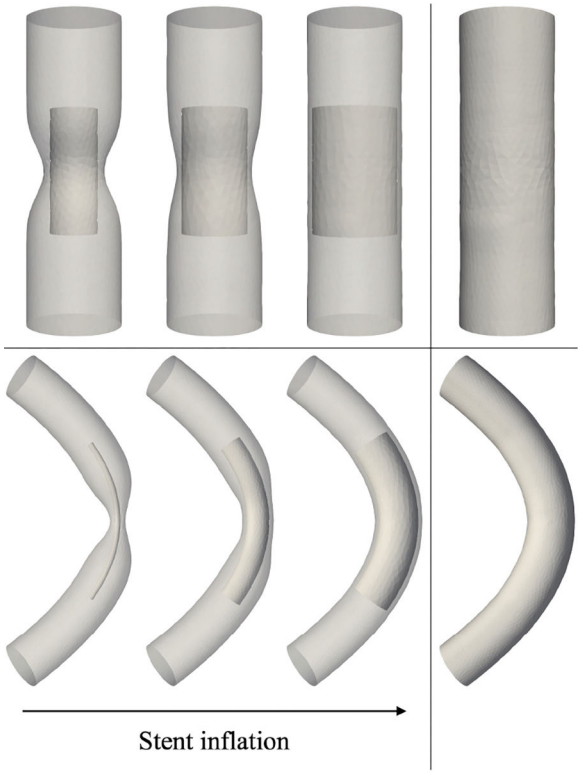

Fig. 4.

The stenosed vessels deform as the embedded stents dynamically inflate, where the top row corresponds to an example of closed-cell stenting in a straight vessel and the bottom row corresponds to an example of open-cell stenting in a curved vessel. The final deformations, corresponding to the stented vessels, are shown in the rightmost column. These results were generated using stiffness values of 10^4, 10^2, and 10^5 for the distance, bending, and vertex-normal collision constraints, respectively.

Author Manuscript Author Manuscript Author Manuscript Author Manuscript

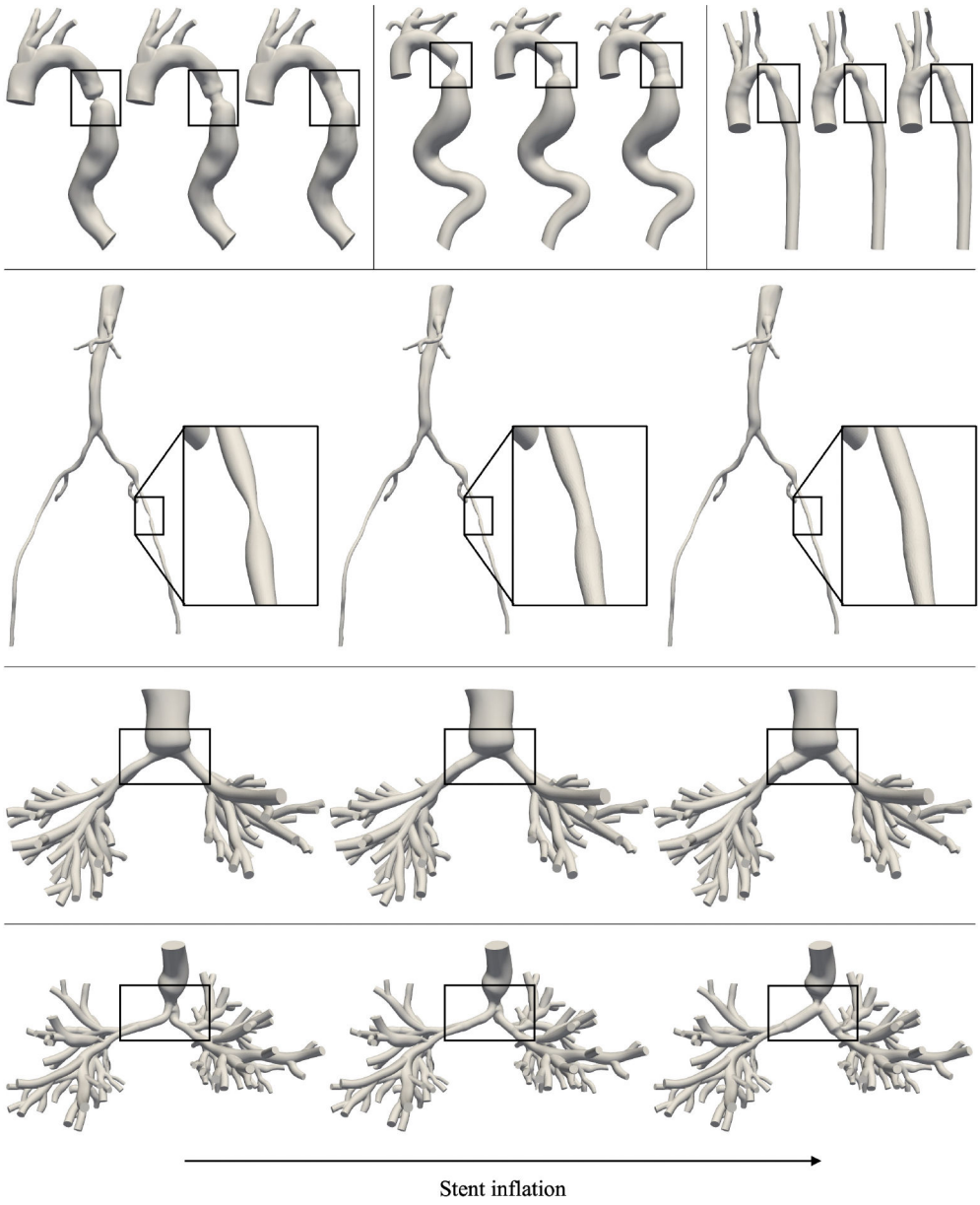

Fig. 5.

Stenting shape edits were performed on six patient-specific models (three aortas, one aortofemoral network, and two pulmonary anatomies). The boxes highlight the location of these shape edits. For each case, we show the vessels at three times during the stenting simulations: input model (left), mid-simulation (middle), and final result (right). Note that the bottom model illustrates closed-cell stenting in curved pulmonary vessels.

Author Manuscript Author Manuscript Author Manuscript Author Manuscript

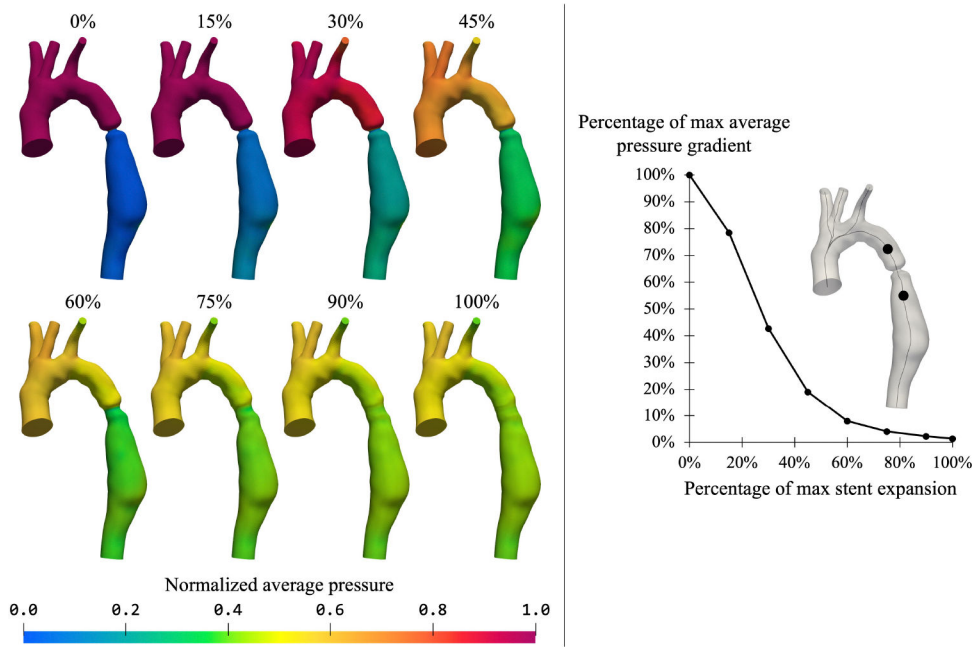

Fig. 6.

A patient-specific aortic coarctation was stented with multiple stent diameters. The percentages displayed above each model correspond to the degree of radial expansion of the stent, relative to the amount of expansion prescribed in the last model (left panel: bottom right). These percentages are the same as the ones on the x-axis on the chart (right panel), which shows the relationship between the average pressure gradient across the stenosis and the stent diameter. The pressure gradient was measured between the two markers indicated on the inset. The percentages on the y-axis correspond to the pressure gradient measured at each stent diameter, relative to the gradient measured in the first model (left panel: top left).

Author Manuscript Author Manuscript Author Manuscript Author Manuscript

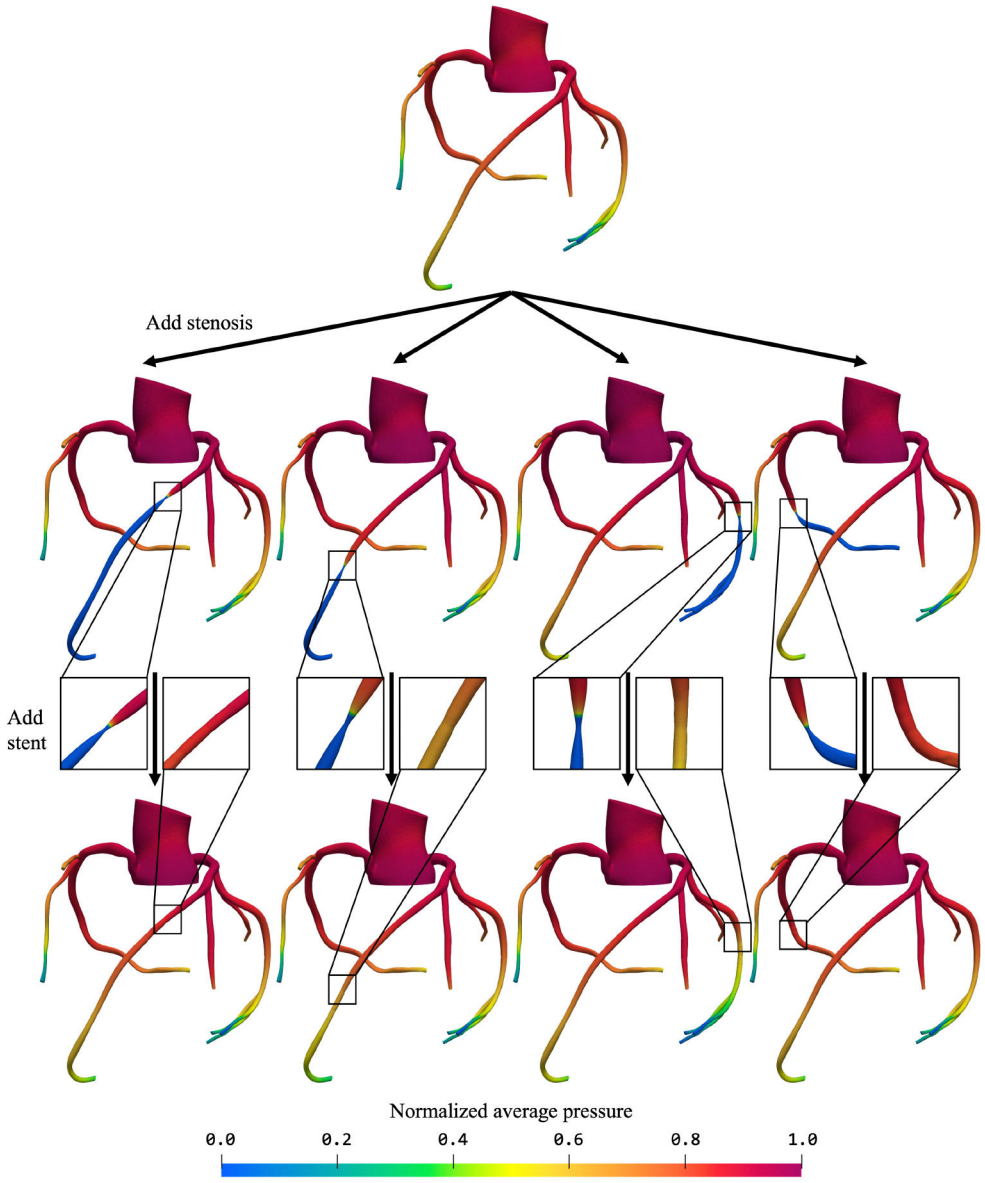

Fig. 7.

An example database of synthetic stenoses (middle row) and stented outcomes (bottom row), with corresponding CFD simulations, was created. The stenoses were generated on a healthy patient-specific coronary model (top row) using a Kelvinlet-based stenosis-generation technique [15].